Sequential Norrish-Yang Cyclization and C–C Cleavage/Cross-Coupling of a [4.1.0] Fused Saturated Azacycle

Charis Amber Roberts,[a, b] Bohyun Park,[a, c] Li-Ping Xu,[d] Jose B. Roque,[a] Charles S. Yeung,[e] Djamaladdin G. Musaev,[d]* Richmond Sarpong,[a]* Rebecca Lyn LaLonde [b]*

[a] Department of Chemistry, University of California, Berkeley, California 94720, United States.

[b] Chemistry Department, Reed College, Portland, Oregon 97202, United States.

[c] Department of Chemistry, Korea Advanced Institute of Science and Technology (KAIST), Daejeon 34141, Republic of Korea.

[d] Cherry L. Emerson Center for Scientific Computation, and Department of Chemistry, Emory University, Atlanta, Georgia 30322, United States.

[e] Disruptive Chemistry Fellow, Department of Discovery Chemistry, Merck & Co., Inc., 33 Avenue Louis Pasteur, Boston, Massachusetts 02115, United States.

Supporting Information Placeholder

ABSTRACT:

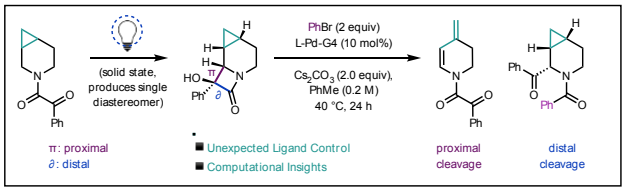

Methods that functionalize the periphery of azaycylic scaffolds have garnered increasing interest in recent years. Herein, we investigate the selectivity of a solid-state Norrish-Yang cyclization (NYC) and subsequent C–C cleavage/cross-coupling reaction of a strained cyclopropane-fused azacyclic system. Surprisingly, the NYC furnished primarily a single lactam constitutional- and diastereo-isomer. By altering the ligand set used in the coupling chemistry, the regioselectivity of C–C cleavage of the α-hydroxy-β-lactam moiety could be varied. Experimental and computational observations are discussed.

Saturated cyclic amines (azacycles) are ubiquitous in natural products, agrochemicals, and pharmaceuticals.[1] Among drugs that are prescribed in the United States, piperidines are the most common azacycle, occurring in over 10% of the 640 heterocycle-containing drugs on the market in 2014.[2] As such, synthetic methods that diversify azacycle-containing compounds in order to access novel scaffolds are of great importance.[3]

In recent years, various transition metal-mediated methodologies for the peripheral functionalization of C(sp^3)–H rich azacycles (Figure 1A) have been reported. For example, Sames and coworkers demonstrated in a single case that the α-arylation of piperidines bearing an N-amidine directing group could be achieved using Ru catalysis with boronate esters as coupling partners.[4] Maes and coworkers disclosed a broader scope for this type of α-arylation using N-pyridyl piperidines under similar conditions, albeit resulting in competing mono- and di- functionalization.[5] More recently, Yu and coworkers,[6,7] Gong and coworkers,[8] as well as Glorius and coworkers,[9] demonstrated enantioselective α-functionalization of a range of azacycles, including piperidines, using thioamide or amidoxime directing groups.

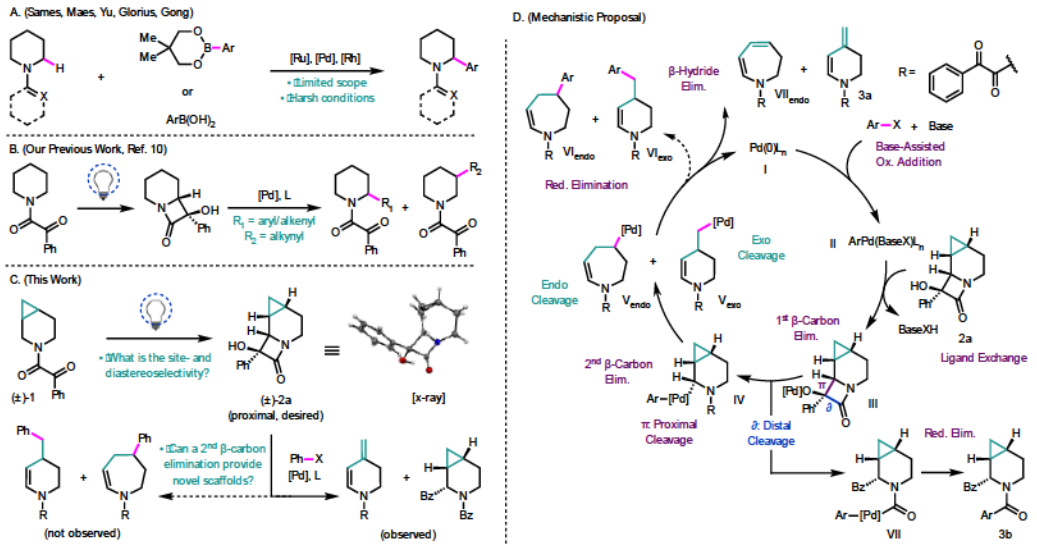

Figure 1. (A) Previous methodologies for the α-functionalization of saturated azacycles. (B) Our recent methodology for the α-functionalization of saturated azacycles. (C) Investigations into the selectivity of the Norrish-Yang cyclization (NYC) and palladium-mediated cleavage/cross-coupling of a cyclopropane-fused piperidine. (D) Mechanistic proposal for the C–C cleavage cross-coupling reaction.

Previously, we described a methodology for the mild functionalization of a variety of saturated azacycles (Figure 1B).[10] Our approach exploited a Norrish-Yang cyclization (NYC) to annulate a highly strained α-hydroxy-β-lactam moiety onto azacyclic scaffolds, setting the stage for a subsequent C–C cleavage/cross-coupling to access both α- and β-functionalized azacyclic products. On the basis of this methodology, we questioned whether azacycles fused to highly strained cyclopropanes would engender an additional β-carbon elimination, providing access to additional novel, value-added, scaffolds (Figure 1 C). Furthermore, this study could provide support for our recent work[11] centered on elucidating the factors that control the regioselectivity of C–C cleavage (i.e., proximal vs. distal; see Figure 1D) using biarylphospine-Pd complexes. Previously, we found that a crucial donor-acceptor interaction between the ligand and the metal controlled the site of C–C cleavage in the α-hydroxy-β-lactam, through what was termed steric enabled electronic effects from the ligand (SEEEL).[11]

Herein, we report studies on the stereo-, chemo-, and diastereoselectivity of the NYC of a cyclopropane-fused piperidinyl ketoamide (**1**; see Figure 1C). A high level of site-, diastereo-, and chemoselectivity was achieved using optimized reaction conditions, leading to the preferential formation of the desired lactam. The Pd-mediated C–C cleavage/cross-coupling reactions of this unique substrate were explored, providing access to novel scaffolds depending on the choice of ligand. Interestingly, a reactivity profile which is complementary to our previous results was observed. Specifically, using APhos as ligand, cleavage of the distal C–C bond of the α-hydroxy-β-lactam occurred preferentially to furnish α-benzoyl piperidinyl amide **3b** (Figure 1D). Using our previously established RuPhos system, proximal C–C bond cleavage was observed. However, under the latter conditions, following C–C bond cleavage, cross-coupling (requiring RE) was not observed and only β-hydride elimination occurred under the various conditions that were screened to give **3a**. Density functional theory (DFT) calculations corroborated this finding and showed that in this system, proximal C–C bond cleavage is kinetically favored, whereas the downstream RE has a significantly high barrier. In contrast, when APhos was used as ligand, a switch in selectivity, also supported by computations, was observed. Specifically, in switching from RuPhos to APhos, we calculated a significant decrease in the $\Delta\Delta G^{\ddagger}$ associated with selectivity for proximal versus distal C–C cleavage, representing a switch in selectivity to distal cleavage under kinetic control. This work extends our previous understanding of the factors that control reactivity and selectivity in these Pd-catalyzed cross-couplings.

STUDIES ON THE NORRISH-YANG CYCLIZATION

At the outset of this work, we recognized that in order for our proposed cyclopropane-cleavage event to proceed, the NYC had to site-selectively functionalize the cyclopropylcarbinyl methylene group. In this way, the α-Pd intermediate that would be generated following an initial β-carbon elimination (see **IV**, Figure 1D) would be poised for cyclopropane cleavage through a subsequent β-carbon elimination. The NYC could also lead to numerous stereoisomers (8 possible lactams). Moreover, as had been observed in our previous studies, there was the potential that an undesired N,O-acetal product (**2b/c**, Table 1, for example) could form instead of the desired lactam, leading to a total of 16 possible isomeric products.

We therefore sought to determine the selectivity of the NYC of cyclopropane-fused piperidinyl ketoamide **1** (see the Supporting Information for preparation). Upon irradiation of the starting ketoamide (**1**) using our previously established conditions (Table 1, entry 1), we observed full consumption of **1** by ^{1}H NMR. We observed a high site-selectivity for the cyclopropylcarbinyl position, and a single lactam diastereomer (**2a**) in 18% yield, the stereochemistry of which was unambiguously determined by single crystal X-ray diffraction (XRD) analysis (Figure 1C). In addition to **2a**, we observed a pair of N,O-acetal diastereomers (**2b/c**) in roughly a 1:1 ratio (combined yield of 17%). The remainder of the mass balance was accounted for by an intractable mixture of decomposition products and/or unidentifiable constitutional isomers. During our optimization studies, we observed that the reaction had progressed to near completion after 1 h on 0.02 mmol (5 mg) scale (entry 2). On this basis, we sought to maximize the surface area for this solid phase reaction setup by using a glass slide as

the reaction vessel, which proved to be crucial to the reaction rate (entry 3). Following literature precedent,[13] we found that cooling the reaction setup (see the Supporting Information for pictures and details of reaction setup) pushed the product distribution toward the desired lactam (entry 4). Ultimately, we observed full consumption of the starting material, as well as an improved product ratio of 1: 0.24, after 5 h (35% isolated yield of lactam) on 0.9 mmol (200 mg) scale at approximately –78 °C.

Table 1. Optimization data for the production of lactam 2a.

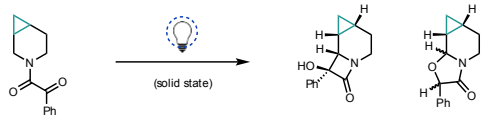

entry	scale (mg)	time (h)	temp. (°C)	method[a]	2a:2b/c[b]
1	200	16	rt	vial	1: 0.95
2	< 5	1	rt	vial	1: 1.1
3	23	0.75	rt	slide	1: 0.56
4	100	4	~ -78	slide w/ N_2 stream	1: 0.22
5	200	5	~ -78	slide w/ N_2 stream	1:0.24

[a]Vial reactions run under N_2 atmosphere. [b]Ratios determined by ^{1}H NMR analysis of the crude reaction mixture.

Previous studies of solid-state Norrish type II processes have shown that factors such as equilibrium geometries of the diradical intermediate,[14, 15] or the presence of intermolecular hydrogen bonds[16] can dictate the stereochemical outcome. We propose, in alignment with the topochemical postulate,[17] that the observed stereoselectivity of this solid state transformation of **1** likely arises from the tendency of crystals to minimize overall reorganization, thus maintaining the greatest level of order in the bulk state. Therefore, it is likely the case that the equilibrium geometry of the crystal lattice of ketoamide **1** leads to one methylene H-atom being accessible with minimal molecular motion. Ultimately, this scenario leads to a stereoselective hydrogen atom transfer (HAT), furnishing a chiral radical center, which, upon recombination, provides the observed product in high diastereoselectivity. Under this mechanistic scenario, more than one N,O-acetal diastereomer is likely, as the C–O radical recombination requires additional molecular motion, which would allow access to other modes of reactivity. This is supported by the observed temperature dependence of the product distribution, wherein entropic factors may play a role in the formation of **2b** or **2c** at increased temperatures, and the fact that the crystal lattice is disrupted upon product formation, leading to melting point depression with reaction progress (the crystalline solid will become an oil if not kept cool as the reaction progresses). Additionally, this hypothesis is supported by single crystal XRD analysis of the starting ketoamide **1** (Table 1), which shows a clear proximity differential between the ketone moiety and the neighboring methylene groups, favoring the observed positional isomers. Moreover, a large difference in proximity between two of the methylene protons at the cyclopropylcarbinyl position (see the Supporting Information for details) provides an explanation for the high level of diastereoselectivity observed in the lactam product. In comparison to archetypical radical clocks, such as the cyclopropyl methyl radical, this places the recombination event on the order of 10^7 s^{-1} or faster,[12] making it competitive with cyclopropane cleavage.

Studies on Subsequent C–C Cleavage/Cross-Coupling

With **2a** in hand, we set out to investigate the C–C bond cleavage/coupling chemistry. Using our previously established cross-coupling conditions, starting lactam **2a** was fully consumed to form two major products, which were identified as **3a** — resulting from sequential C–C cleavage followed by β-hydride elimination — in 60% isolated yield, and α-benzoylated **3b** in 12% isolated yield — resulting from distal C–C cleavage of the α-hydroxy-β-lactam (Table 2; entry 2). The observed products are consistent with the structural constraints inherent in starting lactam **2a**. Given that β-carbon elimination must occur via a four-membered transition state (TS), the forming and breaking bonds must be *syn* disposed. However, on the basis of the stereochemistry of the α-hydroxy-β-lactam in **2a**, only the *exo* cyclopropyl C–C bond can engage in this process, furnishing a 4-(1-methyl)-palladated intermediate (Figure 1D; $\mathbf{V_{exo}}$), setting the stage for the observed β-hydride elimination. This is in contrast to an *endo* cyclopropyl C–C cleavage which would afford the corresponding azepine derivative (Figure 1C; *exo* vs. *endo* cleavage).

Table 2. Investigation into the cross-coupling/cleavage reaction of lactam 2a.

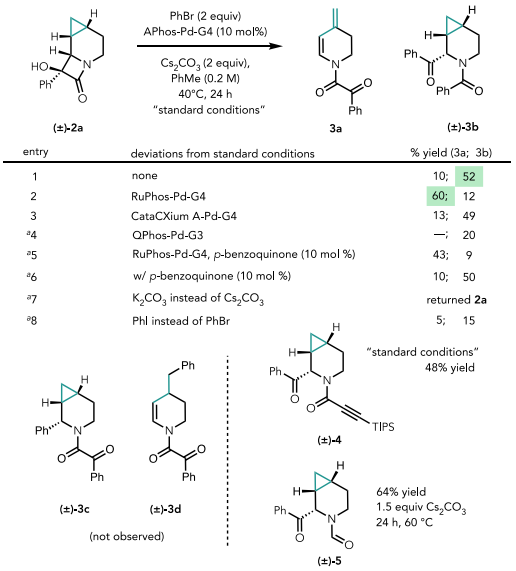

entry	deviations from standard conditions	% yield (3a; 3b)
1	none	10; 52
2	RuPhos-Pd-G4	60; 12
3	CataCXium A-Pd-G4	13; 49
[a]4	QPhos-Pd-G3	—; 20
[a]5	RuPhos-Pd-G4, *p*-benzoquinone (10 mol %)	43; 9
[a]6	w/ *p*-benzoquinone (10 mol %)	10; 50
[a]7	K_2CO_3 instead of Cs_2CO_3	returned **2a**
[a]8	PhI instead of PhBr	5; 15

[a]NMR yield based on ^{1}H NMR integration using 1,3,5-trimethoxybenzene as internal standard. Reactions run on 0.1 mmol scale.

Following these initial observations, we sought conditions to favor reductive elimination (RE) and therefore cross-coupling. Interestingly, with all the ligands that were evaluated using microscale high-throughput experimentation (HTE; see the Supporting Information for a list of ligands screened), we observed exclusive proximal C–C cleavage followed by β-carbon and β-hydride elimination to furnish diene product **3a**, and/or distal C–C cleavage to furnish α-benzoylated benzamide **3b**, with no α-arylated product (**3c**) or cyclopropyl cleavage cross-coupling product (**3d**) observed. Ultimately, we found that with a metal complex bearing a bulky ligand (APhos-Pd-G4, 10 mol%), **3b** could be isolated in 52% yield holding all other conditions constant (Table 2; entry 1). The stereochemistry of **3b** was verified by single crystal XRD analysis (see the Supporting Information). Similar results were

observed using CataCXium A as ligand (entry 3), and although using QPhos proved optimal on analytical scale, this was not the case on 0.1 mmol scale (entry 4), which furnished only 20% of **3b** as a part of a complex mixture, indicative of many competing side reactions. Attempts to favor RE using RuPhos, for example, by the addition of a π-acid (*para*-benzoquinone, 10 mol%), decreased the yield of diene **3a** (entry 5), likewise leading to a complex mixture. Notably, formation of **3d** was still not observed. Finally, addition of π-acids when APhos-Pd-G4 was used as catalyst did not lead to any improvements in selectivity (entry 6).

In alignment with our previous observations, Cs_2CO_3 was shown to be the optimal base for this transformation (entry 7), whereas using K_2CO_3 as base returned the starting lactam. PhI proved to be significantly less efficient as an aryl source (entry 8), resulting in 35% recovered starting lactam. Interestingly, alkynylated amide **4** — the structure of which was confirmed by single crystal XRD analysis — was isolated in 48% yield under these optimized conditions as a single diastereomer when (bromoethynyl)triisopropylsilane was used as the coupling partner. Finally, when **2a** was subjected to our previously established protocol for the conversion of azacycles to the corresponding α-benzoyl-N-formyl derivatives,[10] we obtained α-keto aza-bicycloheptanyl formamide **5** in 64% isolated yield as a single diastereomer (verified by single crystal XRD analysis).

Computational Investigations of the Cross-Coupling Ligand Effects

To better understand the role of the ligand in determining the product distribution, we conducted density functional theory (DFT) calculations (see the Supporting Information for figures and a full analysis). Using RuPhos, our calculations indicate that cleavage of the proximal C–C bond cleavage is more favorable, with a free energy barrier of 10.60 kcal/mol, whereas the distal cleavage has an activation free energy of 14.05 kcal/mol (see Figure S13). The calculated preference for proximal C–C bond cleavage over distal C–C bond cleavage of the β-lactam using the RuPhos-ligated Pd(II)-complex is consistent with our previous computational findings and the experimental observations presented above. [10, 11, 18]

In contrast, using monodentate phosphine ligands CataCXium A or APhos, we observed a reversal in the distal/proximal C–C cleavage selectivity leading to α-benzoylated species **3b** as a major product. Specifically, the product ratio reversed by a factor of 26 (Table 2, entries 1, 2) upon switching from RuPhos to APhos. This experimental observation is in full agreement with our previous findings[11] and corresponds to a 2 kcal/mol calculated difference between the free energy barriers of distal and proximal cleavage in comparing RuPhos to APhos or to CataCXiumA. Calculations for the C–C bond cleavage steps using APhos and CataCXium A as ligands (see Figure S14) revealed $\Delta\Delta G^{\ddagger}$ values of 0.61 and 0.52 kcal/mol, for APhos and CataCXium, respectively, showing a clear decrease of approximately 3 kcal/mol in selectivity to favor distal cleavage compared to the RuPhos case ($\Delta\Delta G^{\ddagger}$ = 3.45 kcal/mol); in full agreement with experiment. Additionally, the above presented distal/proximal selectivity data for the RuPhos, APhos, and CataCXium A ligated systems are consistent with a distortion-interaction analysis,[22, 23] details of which can be found in the Supporting Information.

Conclusion

In conclusion, for highly strained, cyclopropane-fused piperidinyl ketoamide **1**, the Norrish Yang Cyclization (NYC) to form the corresponding α-hydroxy-β-lactam proceeds in a highly chemo-, diastereo- and site-selective fashion under the optimized conditions. A C–C bond cleavage/cross-coupling reaction using this substrate provided access to unusual scaffolds such as **3a**, **3b**, and **4**. DFT calculations revealed that in the case of RuPhos, the desired reactivity for the formation of **3c** or **3d** was hampered by a rapid β-hydride elimination. In contrast, monodentate ligands APhos and CataCXiumA favored distal C–C bond cleavage. The empirical observations of the product distribution in the solid-state photoreaction of **1** are currently being computationally investigated and will be disclosed in due course.

Experimental Section

General Unless otherwise stated, all reactions were performed in flame-dried or oven-dried glassware under an atmosphere of nitrogen with Teflon coated stir bars. Photochemical reactions were conducted using a 40 W Kessil A160WE Blue LED 400-450 nm fixed wavelength lamp. Reactions performed at elevated temperatures were heated in an oil bath; room temperature is defined as 23 °C. All commercially available reagents were used without purification. Flash column chromatography was performed with Silicycle SiliaFlash P60 silica gel (230−400 mesh, 40−63 μm particle size). $AgNO_3$-impregnated (10 % w/w) silica was purchased from Silicycle. Compounds were visualized with UV light (254 nm) and stained with *p*-anisaldehyde and heat, or potassium permanganate ($KMnO_4$) and heat. TLC and preparative TLC were performed on glass-backed Silicycle SiliaPlate 250 μm thickness, 60 Å porosity F-254 precoated plates. $AgNO_3$-impregnated TLC plates were prepared by running a 10% w/v solution of $AgNO_3$ in MeCN to the top of the glass-backed Silicycle SiliaPlate 250 μm thickness, 60 Å porosity F-254 precoated plates, then drying the plates in an oven at 160 °C for 10 minutes. They were wrapped in foil and stored away from light when not in use. Automated flash chromatography was performed on Yamazen Flash EPCLC W-Prep 2XY (dual channel) automated flash chromatography systems with premium grade universal columns. Microwave reactions were conducted using a Biotage Initiator + ™ microwave reactor. All microwave reactions were conducted in sealed microwave vials provided by the manufacturer. Reactions progress was monitored by thin layer chromatography (TLC). Nuclear magnetic resonance (NMR) spectra were obtained on Bruker AV-300 (NSF Grant CHE-0130862 and NSF Grant CHE-911557), AVQ400 (NSF Grant CHE-0130862), AVB-400 (NSF Grant CHE0130862, NIH Grant S10 RR 03353-01, and NSF Grant CHE8703048), AV-500 (NIH Grant 1S10RR016634-01), and AV600 (NIH Grant SRR023679A) instruments at UC Berkeley's College of Chemistry NMR Facility. Residual solvent was used as internal reference ($CDCl_3$, 7.26 ppm; C_6D_6, 7.17 ppm). The following abbreviations were used to describe the NMR multiplicities: br = broad, s = singlet, d = doublet, t = triplet, q = quartet, q = quintet, m = multiplet. Coupling constants *J* are given in Hertz. High-resolution mass spectra (HRMS) were obtained on a PerkinElmer AxION 2 UHPLC-TOF Instrument (ESI). Melting point data were collected on an Mel-Temp II melting point apparatus. IR data were collected on a Bruker Vertex 80 FTIR spectrometer. Single crystal XRD measurements were performed on a Rigaku XtaLAB P200 equipped with a MicroMax 007HF rotating anode and a Pilatus 200K hybrid pixel array detector.

EXPERIMENTAL PROCEDURES

Starting Material Preparation

N-Boc 3-azabicyclo[4.1.0]heptane (**S1**)

A solution of diethyl zinc (1.0 M in hexanes, 40 mL, 40 mmol, 4 equiv) was added dropwise via syringe to a solution of CH_2Cl_2 (50 mL) at 0 °C. under a flow of N_2. A solution of TFA (3.2 mL, 40 mmol, 4.0 equiv) in CH_2Cl_2 (10 mL) was then added dropwise via syringe, and the mixture was stirred for 40 min at 0 °C. After this time, a solution of CH_2I_2 (3.0 mL, 40 mmol, 4.0 equiv) in CH_2Cl_2 (10 mL) was added dropwise via syringe. 10 mL of air then was injected using a syringe. The reaction mixture was stirred for an additional 40 min. A solution of N-Boc-1,2,3,6-tetrahydropyridine (1.8 mL, 10 mmol, 1 equiv) in CH_2Cl_2 (30 mL) was then added dropwise to the reaction mixture via cannula, and the reaction mixture was allowed to warm to room temperature and stirred for 12 h. The reaction mixture was cooled in an ice bath, and Et_3N (1.7 mL, 12 mmol, 1.2 equiv) and Boc_2O (2.4 g, 11 mmol, 1.1 equiv) were added sequentially and the mixture was stirred at room temperature for 12 h. Another 1.09 g (5.0 mmol, 0.50 equiv) of Boc_2O was then added and the mixture was stirred for an additional 12 h. After this time, the reaction mixture was quenched with sat. aq. NH_4Cl (40 mL), the organic layer was separated, and the aqueous phase was extracted with CH_2Cl_2 (3 X 50 mL). The organic layers were combined, dried over $NaSO_4$, and concentrated in vacuo to yield a reddish oil. The crude material was purified in stages using normal phase silica gel column chromatography (0 to 20% EtOAc/hexanes), followed by $AgNO_3$-impregnated Silica column chromatography (8 mL of $AgNO_3$-SiO_2 per 100 mg of crude material; eluting with 4 column volumes each of 0%, 0.5%, 1.0%, and 1.5% MTBE/pentane followed by an additional 12 column volumes of 1.5% MTBE/pentane), furnishing **S1** as a translucent, light-yellow oil with a floral scent (0.97 g, 49% yield). **^{1}H NMR** (400 MHz, $CDCl_3$) δ 3.71 (dd, *J* = 13.3, 1.3 Hz, 1H), 3.52 (dd, *J* = 13.4, 3.7 Hz, 1H), 3.29 (m, 1H), 2.98 (ddd, *J* = 13.6, 8.7, 5.4 Hz, 1H), 2.00 – 1.79 (m, 1H), 1.66 (m, 1H), 1.45 (s, 9H), 0.97 (s, 2H), 0.61 (td, *J* = 8.6, 4.9 Hz, 1H), 0.13 (q, *J* = 5.1 Hz, 1H). **^{13}C{^{1}H} NMR** (100 MHz, $CDCl_3$) δ 155.2, 79.2, 42.2, 40.3, 28.5, 22.7, 9.6, 8.9, 7.9. **IR** (neat): 1688 (s) cm^{-1}. **HRMS** (ESI): calculated for $C_{11}H_{19}NO_2$ [M+Na]$^+$: 220.1308, found: 220.1308.

1-(3-azabicyclo[4.1.0]heptan-3-yl)-2-phenylethane-1,2-dione (**1**) A medium microwave vial was charged with N-Boc 3-azabicyclo[4.1.0]heptane (**S1**, 269 mg, 1.37 mmol, 1.00 equiv) and anhydrous 1M Et_2O•HCl (7.0 mL, 8.8 mmol, 8.0 equiv). The vial was equipped with a stir bar and fitted with a vial adapter and cap. The mixture was heated in a microwave at 100 °C for 6 min (0 bar additional pressure; absorption level set to "Normal"). The pressure of the reaction vessel increased upon heating to the reaction temperature and stabilized at 8 bar for the duration of heating. At the end of the heating period, a fluorescent yellow precipitate had formed that coated the walls of the vial, and a yellow oil had collected at the bottom of the vial. The vial was cooled to room temperature and vented using a needle, then was uncapped and the contents concentrated under a stream of nitrogen. The residue was dissolved in a minimal amount of CH_2Cl_2 (<5 mL), and Et_2O (~10 mL) was added, which led to the formation of light yellow, off-white crystals. The solvent was evaporated under a stream of nitrogen, and the resulting crystals were dried in vacuo. This resulting material was used in the following step without further purification .

Benzoylformic acid (254 mg, 1.69 mmol, 1.00 equiv) and CH_2Cl_2 (30 mL) were added to an oven-dried 100 mL flask equipped with a magnetic stir bar under flow of N_2. The resulting light-yellow solution was stirred for 5 min, at which point oxalyl chloride (0.146 mL, 1.69 mmol, 1.00 equiv) was added. The solution was stirred for 10 min at room temperature, followed by the addition of one drop of anhydrous DMF, at which point the solution grew darker in color. Evolving HCl gas was bubbled through a 1M solution of NaOH, and the reaction mixture was stirred under N_2 until bubbling had ceased (approx. 3 h). The solution was then cooled to 0 °C, and the crystalline material produced in the prior step above (182 mg, 1.36 mmol, 0.800 equiv) was added, followed by Et_3N (0.354 mL, 2.54 mmol, 1.50 equiv). The reaction mixture was stirred at room temperature for 16 h, and then was quenched with 20 mL H_2O and the layers were separated. The aqueous phase was extracted with CH_2Cl_2 (3 X 20 mL) and the organic extracts were combined, dried over Na_2SO_4, and concentrated in vacuo to give a yellow oil. Purification of the crude material by column chromatography (Silica, 0 to 10% EtoAc/Hexanes) provided the title compound as a colorless oil, which was crystallized using ice cooled pentane (250 mg, 80% yield, mixture of rotamers 1: 0.5). Alternatively, addition of a seed crystal and putting the material under a vacuum yields the crystalline material. Single crystals for XRD analysis were grown by slow evaporation of a supersaturated solution of the ketoamide (**1**) (50 mg) in hot HPLC grade hexanes (~2 mL). **^{1}H NMR** (400 MHz, $CDCl_3$) δ 7.94 (ddd, *J* = 8.6, 5.4, 1.3 Hz, 1H), 7.65 (dddd, *J* = 8.7, 5.5, 2.8, 1.4 Hz, 1H), 7.55 – 7.48 (m, 1H), 4.10 (dd, *J* = 13.7, 1.6 Hz, 0.5H), 3.86 (dd, *J* = 13.7, 5.5 Hz, 0.5H), 3.83 – 3.76 (m, 0.5H), 3.67 (dd, *J* = 13.5, 4.9 Hz, 0.5H), 3.51 (dd, *J* = 13.4, 2.0 Hz, 0.5H), 3.22 (ddd, *J* = 13.2, 9.2, 5.6 Hz, 0.5H), 3.11 (m, 1H), 2.13 (ddt, *J* = 14.2, 7.3, 5.5 Hz, 1H), 1.98 (ddt, *J* = 11.5, 6.9, 5.7 Hz, 1H), 1.85 (dddd, *J* = 14.6, 8.9, 5.8, 2.6 Hz, 0.5H), 1.73 (dtd, *J* = 14.0, 7.1, 6.6, 2.1 Hz, 1H), 1.21 – 1.06 (m, 1H), 0.99 (dddd, *J* = 13.7, 8.6, 5.3, 2.1 Hz, 0.5H), 0.80 (td, *J* = 8.8, 5.2 Hz, 0.5H), 0.71 (td, *J* = 8.7, 5.2 Hz, 0.5H), 0.32 (dq, *J* = 8.6, 5.3 Hz, 1H) (8 ^{1}H resonances overlap due to amide rotation). **^{13}C{^{1}H} NMR** (126 MHz, $CDCl_3$) δ 191.67, 191.66, 166.3, 166.0, 134.7, 133.2, 133.1, 129.7, 129.0, 128.98, 44.6, 42.3, 40.141, 38.5, 23.5, 22.4, 9.7, 9.6, 9.4, 9.2, 8.1, 7.8 (2 ^{13}C resonances overlap due to amide rotation). **IR** (neat): 1677 (s), 1632 (s) cm^{-1}. **Mp**: 64–67 °C. **HRMS** (ESI): calculated for $C_{14}H_{15}NO_2$ [M+Na]$^+$: 252.0995, found: 252.0994.

Low-Temperature Reaction Setup On a glass plate (4 cm X 4 cm X 1 mm) was placed **1** (205 mg, 0.890 mmol), previously chopped to a fine consistency with a razor blade, which was secured by placing an additional glass plate of the same size on top, the edges of which were sealed with electrical tape and secured on a ring stand 1 cm above a 40 W Kessil A160WE Blue LED 400-450 nm fixed wavelength lamp (Figure S1, top left). A crystallization dish filled with dry ice (left out for photos) and iPrOH and covered with aluminum foil was placed on the surface the glass side, with a nitrogen stream running over the bottom face of the plate (Figure S1, top right). The LED Kessil lamp was turned on full intensity (Figure S1, bottom left) and a bucket was placed over the reaction set up (Figure S1, bottom right) to minimize exposure to the light. (see the supporting information for details).

1S,2R,4R,9S)-9-Hydroxy-9-phenyl-7-azatricyclo[5.2.0.02,4]nonan-8-one (**2a**). Compound **2a** was prepared according to the procedure outlined in "Low Temperature Photoreaction Setup" (see the Supporting Information for pictures and details). After 5 h, completion of

the reaction was determined by NMR analysis, the material was transferred to a 20 mL scintillation vial using CH_2Cl_2. Several reaction runs (4x205 mg) were combined (total crude mass of 820 mg) and purified using column chromatography (silica, 0 to 60% EtOAc/hexanes). Further purification using column chromatography (silica, 0 to 40% Et_2O/hexanes) provided **2a** as a white crystalline solid (376 mg, 35% yield). Single crystals for XRD analysis were grown by slow evaporation of a solution of **2a** (<3 mg) in HPLC-grade EtOAc (<1 mL). **^{1}H NMR** (400 MHz, $CDCl_3$) δ 7.60 – 7.45 (m, 2H), 7.45 – 7.31 (m, 3H), 4.23 (d, *J* = 2.3 Hz, 1H), 3.34 (td, *J* = 12.6, 6.8 Hz, 1H), 3.23 (ddd, *J* = 12.6, 7.4, 1.7 Hz, 1H), 2.83 (s, 1H), 2.10 (tdd, *J* = 12.4, 7.6, 2.5 Hz, 1H), 1.85 (dddd, *J* = 14.4, 6.8, 3.2, 1.8 Hz, 1H), 1.08 – 0.88 (m, 2H), 0.17 (q, *J* = 5.4 Hz, 1H), 0.02 (td, *J* = 8.2, 6.2 Hz, 1H). **^{13}C{^{1}H} NMR** (100 MHz, $CDCl_3$) δ 169.2, 136.5, 128.5, 128.3, 127.6, 88.8, 60.8, 35.4, 17.8, 11.6, 8.8, 2.3. **IR** (thin-film): 3340 (b), 1730 (s) cm^{-1}. **Mp**: 144–147 °C. **HRMS** (ESI): calculated for $C_{14}H_{15}NO_2$ [M+H]$^+$: 230.1176, found: 230.1177.

(2S,6aS,7aS,7bS)-2-Phenylhexahydrocyclopropa[c]oxazolo[3,2-a]pyridin-3(2H)-one (**2b**). Compound **2b** was isolated as a colorless residue in 5% yield (42 mg) using column chromatography (silica, 0 to 60% EtOAc/hexanes) as a side product of the reaction that yielded **2a**. **^{1}H NMR** (500 MHz, $CDCl_3$) δ 7.41 – 7.35 (m, 2H), 7.30 – 7.27 (m, 2H), 7.25 – 7.19 (m, 1H), 5.74 (dd, *J* = 3.4, 2.4 Hz, 1H), 5.19 (d, *J* = 2.4 Hz, 1H), 3.64 (ddd, *J* = 13.4, 7.3, 4.9 Hz, 1H), 2.85 (ddd, *J* = 13.4, 8.7, 6.7 Hz, 1H), 1.90 (dtd, *J* = 14.4, 6.7, 4.9 Hz, 1H), 1.76 – 1.68 (m, 1H), 1.37 (tdd, *J* = 8.6, 5.2, 3.5 Hz, 1H), 1.32 – 1.25 (m, 1H), 0.74 (td, *J* = 8.5, 5.6 Hz, 1H), 0.39 (q, *J* = 5.5 Hz, 1H). **^{13}C{^{1}H} NMR** (126 MHz, $CDCl_3$) δ 169.3, 136.9, 128.8, 128.5, 128.5, 126.1, 86.8, 79.4, 37.3, 20.3, 15.7, 11.5, 7.1. **IR** (thin-film): 1707 (s) cm^{-1}.
HRMS (ESI): calculated for $C_{14}H_{15}NO_2$ [M+H]$^+$: 230.1176, found: 230.1177.

(2R,6aS,7aS,7bS)-2-Phenylhexahydrocyclopropa[c]oxazolo[3,2-a]pyridin-3(2H)-one (**2c**). Compound **2c** was isolated in 5% yield (41 mg) as a colorless residue using column chromatography (silica, 0 to 60% EtOAc/hexanes) as a side product of the reaction that yielded **2a**. **^{1}H NMR** (500 MHz, $CDCl_3$) δ 7.50 – 7.45 (m, 2H), 7.43 – 7.36 (m, 2H), 7.35 – 7.31 (m, 1H), 5.71 (dd, *J* = 3.5, 2.0 Hz, 1H), 5.20 – 5.18 (m, 1H), 2.05 (dtd, *J* = 14.3, 6.6, 5.3 Hz, 1H), 1.79 (dddd, *J* = 14.3, 8.2, 7.3, 2.5 Hz, 1H), 1.52 (tdd, *J* = 8.5, 5.2, 3.4 Hz, 1H), 1.45 – 1.34 (m, 1H), 0.84 (td, *J* = 8.4, 5.5 Hz, 1H), 0.53 (q, *J* = 5.5 Hz, 1H). **^{13}C{^{1}H} NMR** (126 MHz, $CDCl_3$) δ 169.3, 136.4, 128.6, 128.6, 126.9, 85.7, 79.4, 37.4, 20.5, 15.5, 11.5, 7.1. **IR** (thin-film): 1736 (s) cm^{-1}. **HRMS** (ESI): calculated for $C_{14}H_{15}NO_2$ [M+H]$^+$: 230.1176, found: 230.1177.

Representative procedure for C–C cleavage/cross-coupling

((1R,2S,6R)-3-Azabicyclo[4.1.0]heptane-2,3-diyl)bis(phenylmethanone) (**3b**) To an oven-dried 1 dram vial charged with a stir bar was added lactam **2a** (22.9 mg, 0.100 mmol, 1.00 equiv). The vial was brought into a water and oxygen-free glove box and PhBr (31.4 mg, 0.200 mmol, 2.00 equiv) was added, followed by Cs_2CO_3 (65.4 mg, 0.200 mmol, 2.00 equiv), APhos-Pd-G4 (6.5 mg, 10 mol%, 0.1 equiv) and toluene (0.5 mL; previously degassed by consecutive freeze-pump-thaw cycles until no bubbles of gas were observed, and stored over activated molecular sieves). The vial was sealed with Teflon tape and placed in a heating block at 40 °C for 24 h. After this time, the reaction mixture was cooled to rt and filtered through a glass pipette packed with celite. The vial and celite plug were subsequently rinsed with 5% MeOH/CH_2Cl_2 (3 X 1 mL). The resulting crude material obtained after concentration of the filtrate was purified by PTLC (silica, 20% EtOAc/hexanes) to afford **3b** as an opaque white residue (15.9 mg, 52%, mixture of rotamers 1:0.2). Single crystals for XRD analysis were grown by slow evaporation of a solution of **3b** (< 3 mg) in HPLC-grade EtOAc (< 1 mL). **^{1}H NMR** (500 MHz, $CDCl_3$) δ 8.07 (d, *J* = 7.5 Hz, 2 + 0.2H), 7.58 (q, *J* = 7.5 Hz, 1 + 0.2H), 7.51 (t, *J* = 7.6 Hz, 2 + 0.4H), 7.46 (dd, *J* = 6.7, 3.0 Hz, 2 + 0.2H), 7.41 (dd, *J* = 5.2, 1.9 Hz, 3 + 0.4H), 6.31 (d, *J* = 8.8 Hz, 1H), 5.50 (d, *J* = 9.0 Hz, 0.2H), 4.62 (dd, *J* = 13.9, 4.1 Hz, 0.2H), 3.59 (ddd, *J* = 14.2, 5.3, 2.3 Hz, 1H), 3.13 (td, *J* = 13.7, 3.1 Hz, 1H), 2.86 (td, *J* = 13.5, 2.5 Hz, 0.2H), 2.03 (tt, *J* = 13.3, 4.9 Hz, 1 + 0.2H), 1.83 (d, *J* = 14.1 Hz, 0.2H), 1.75 (dt, *J* = 13.9, 2.9 Hz, 1H), 1.51 (qd, *J* = 8.7, 5.2 Hz, 1 + 0.2H), 1.31 (tq, *J* = 15.4, 10.3, 7.8 Hz, 2 + 0.4H), 0.88 (t, *J* = 6.9 Hz, 0.2H), 0.49 (td, *J* = 8.7, 5.6 Hz, 1H), 0.46 – 0.40 (m, 0.2H), 0.39 (q, *J* = 5.6 Hz, 1H), 0.34 (q, *J* = 5.6 Hz, 0.2H) (8 ^{1}H resonances overlap due to amide rotation). **^{13}C{^{1}H} NMR** (126 MHz, $CDCl_3$) δ 197.26, 171.16, 135.86, 135.59, 133.12, 129.58, 128.69, 128.63, 128.51, 128.42, 127.83, 127.00, 126.50, 53.01, 40.56, 40.54, 11.11, 11.02, 10.83, 10.81, 5.29, 5.24. (10 ^{13}C resonances overlap due to amide rotation). **IR** (thin-film): 1689 (s), 1627 (s) cm^{-1}. **Mp**: 120–122 °C. **HRMS** (ESI): calculated for $C_{20}H_{19}NO_2$ [M+Na]$^+$: 328.1308, found: 328.1309.

1-(4-Methylene-3,4-dihydropyridin-1(2H)-yl)-2-phenylethane-1,2-dione (**3a**). The title compound was prepared using a procedure analogous to the Representative Procedure for the formation of **3b** using RuPhos-Pd-G4 (8.5 mg, 10 mol%) as the ligand–precatalyst complex. The reaction mixture was filtered over a plug of celite, eluting with EtOAc in order to avoid decomposition of the title compound. The crude material was purified by preparative TLC (silica, 20% EtOAc/hexanes) to afford **3a** as a yellow residue (13.6 mg, 60%, mixture of rotamers 1:0.75). Note: the title compound is extremely unstable in the solid state and spontaneously polymerizes upon concentration to dryness. **^{1}H NMR** (600 MHz, C_6D_6) δ 7.97 – 7.90 (m, 2H + 1.5H), 7.37 (dd, *J* = 8.2, 1.5 Hz, 0.75H), 7.05 (tt, *J* = 7.5, 4.1, 1.2 Hz, 1H + 1H), 6.99 – 6.94 (m, 2H + 1.5H), 6.31 (dd, *J* = 8.1, 1.5 Hz, 1H), 5.46 (d, *J* = 8.2 Hz, 0.75H), 5.12 (d, *J* = 8.1 Hz, 1H), 4.68 (d, *J* = 1.7 Hz, 0.75H), 4.64 (d, *J* = 1.5 Hz, 1H), 4.46 (t, *J* = 1.7 Hz, 1H), 4.43 (p, *J* = 1.7 Hz, 0.75H), 3.66 – 3.58 (m, 2H), 3.14 – 3.07 (m, 1.5H), 2.00 (tt, *J* = 6.5, 1.6 Hz, 2H), 1.88 (tt, *J* = 6.5, 1.6 Hz, 1.5H). **^{13}C{^{1}H} NMR** (151 MHz, C_6D_6) δ 190.4, 190.1, 164.8, 163.7, 137.4, 137.3, 134.2, 134.2, 133.5, 129.6, 129.6, 128.8, 128.8, 124.8, 123.5, 113.7, 111.9, 111.0, 110.8, 43.7, 39.6, 29.3, 28.6. **IR** (thin-film): 1705 (s), 1612 (s) cm^{-1}. **HRMS** (ESI): calculated for $C_{14}H_{14}NO_2$ [M+H]$^+$: 228.0984, found: 228.0987.

1-((1R,2S,6R)-2-Benzoyl-3-azabicyclo[4.1.0]heptan-3-yl)-3-(triisopropylsilyl)prop-2-yn-1-one (**4**) The title compound was prepared using a procedure analogous to the representative procedure for the formation of **3b** but using (bromoethynyl)triisopropylsilane as the cross coupling partner (52 mg, 0.2 mmol, 2 equiv). The crude material was purified by PTLC (silica, 5% EtOAc/hexanes) to provide **4** as a white residue (19.8 mg, 48% yield) (rotamers 1: 0.3). Single crystals for XRD analysis were grown from slow evaporation of a solution of **4** (< 3 mg) in HPLC-grade EtOAc (< 1 mL). **^{1}H NMR** (500 MHz, $CDCl_3$) δ 8.01 (dt, *J* = 8.3, 1.2 Hz, 2 + 0.6H), 7.61 – 7.55 (m, 1 + 0.3H), 7.48 (dd, *J* = 8.3, 7.0 Hz, 2 + 0.6H), 6.20 (d, *J* = 9.1 Hz, 0.3H), 6.16 (d, *J* = 8.6 Hz, 1H), 4.46 (ddd, *J* = 14.2, 5.6, 2.7 Hz, 0.3H), 4.36 (ddd, *J* = 14.2, 5.5, 2.2 Hz, 1H), 3.23 (td, *J* = 13.6, 3.2 Hz, 1H), 2.75 (td, *J* = 13.2, 3.4 Hz, 0.3H), 2.05 (tq, *J* = 14.3, 4.7 Hz, 1H), 2.01 – 1.92 (m, 0.3H),

1.86 (ddt, J = 13.5, 3.8, 2.1 Hz, 1H), 1.78 (dq, J = 13.7, 3.0 Hz, 0.3H), 1.55 (qd, J = 8.8, 5.2 Hz, 0.3H), 1.42 (qd, J = 8.7, 5.2 Hz, 1H), 1.36 – 1.20 (m, 2 + 0.6H), 1.16 – 1.06 (m, 18H), 0.97 – 0.87 (m, 5.5H), 0.49 (dtd, J = 17.6, 8.7, 5.7 Hz, 1 +0.3H), 0.39 (q, J = 5.6 Hz, 1H), 0.32 (q, J = 5.5 Hz, 0.3H) (6 ^{1}H resonances overlap due to amide rotation). **^{13}C{^{1}H} NMR** (126 MHz, $CDCl_3$) δ 196.5, 195.6, 153.4, 153.2, 135.4, 134.7, 133.4, 133.2, 128.7, 128.5, 128.5, 98.3, 97.6, 95.2, 94.7, 57.1, 52.5, 40.1, 34.2, 22.6, 21.7, 18.5, 18.41, 18.37, 11.85, 11.77, 11.5, 11.4, 11.1, 11.06, 11.02, 10.97, 10.9, 5.98, 5.94, 5.2, 5.1. (1 pair of ^{13}C resonances overlap due to amide rotation. **IR** (thin-film): 1693 (s), 1621 (s) cm^{-1}. **Mp**: 90–93 °C. **HRMS** (ESI): calculated for $C_{25}H_{35}NO_2Si$ $[M+Na]^+$: 432.2332, found: 432.2333.

(1R,2S,6R)-2-Benzoyl-3-azabicyclo[4.1.0]heptane-3-carbaldehyde (**5**) The title compound was prepared according to a literature procedure.[10] The crude material was purified using PTLC (silica, 20% EtOAc/hexanes) to provide **5** as a white residue (14.4 mg, 63% yield; 1: 0.1 mixture of rotamers). Single crystals for XRD analysis were grown from slow evaporation of a solution of **5** (<3 mg) in HPLC-grade EtOAc (< 1 mL). **^{1}H NMR** (500 MHz, $CDCl_3$) δ 8.10 (s, 1 + 0.1H), 8.03 – 7.99 (m, 2 + 0.2H), 7.58 (tt, J = 6.9, 1.2 Hz, 1 + 0.1H), 7.51 – 7.46 (m, 2 + 0.2H), 6.04 (d, J = 8.6 Hz, 1H), 5.41 (d, J = 9.0 Hz, 0.1H), 4.30 (ddd, J = 14.1, 5.7, 1.9 Hz, 0.1H), 3.48 (ddd, J = 14.0, 5.5, 2.1 Hz, 1H), 3.21 (td, J = 13.5, 3.6 Hz, 1H), 2.71 (td, J = 13.5, 3.6 Hz, 0.1H), 1.99 (tt, J = 13.1, 5.0 Hz, 1H), 1.90 (ddt, J = 13.4, 3.8, 1.9 Hz, 1H), 1.80 – 1.74 (m, 0.1H), 1.53 (qd, J = 8.8, 5.2 Hz, 0.1H), 1.43 (qd, J = 8.7, 5.3 Hz, 1H), 1.32 (dqt, J = 11.6, 4.5, 2.2 Hz, 1H), 0.55 – 0.45 (m, 1 + 0.1H), 0.37 (qd, J = 5.6, 2.2 Hz, 1H), 0.34 – 0.29 (m, 0.1H) (5 ^{1}H resonances overlap due to amide rotation). **^{13}C{^{1}H} NMR** (126 MHz, $CDCl_3$) δ 196.3, 161.7, 135.2, 133.3, 128.9, 128.7, 128.5, 128.4, 56.2, 51.5, 39.2, 32.9, 22.8, 21.5, 11.8, 11.7, 11.44, 11.43, 10.6, 10.5, 6.2, 5.0 (2 ^{13}C resonances overlap due to amide rotation). **IR** (thin-film): 1693 (s), 1662 (s) cm^{-1}. **Mp**: 92–95 °C. **HRMS** (ESI): calculated for $C_{14}H_{15}NO_2$ $[M+H]^+$: 230.1176, found: 230.1179.

ASSOCIATED CONTENT

Supporting Information

The Supporting Information is available free of charge on the ACS Publications website.

Experimental procedures, computational details, and compound characterization (PDF)
X-ray data for compound **1** (CIF)
X-ray data for compound **2a** (CIF)
X-ray data for compound **3b** (CIF)
X-ray data for compound **4** (CIF)
X-ray data for compound **5** (CIF)

AUTHOR INFORMATION

Corresponding Authors

Rebecca Lyn LaLonde – Chemistry Department, Reed College, Portland, Oregon 97202, United States. *rlalonde@reed.edu

Richmond Sarpong – Department of Chemistry, University of California, Berkeley, California 94720, United States.
*rsarpong@berkeley.edu

Djamaladdin G. Musaev – Cherry L. Emerson Center for Scientific Computation, and Department of Chemistry, Emory University, Atlanta, Georgia 30322, United States.
*dmusaev@emory.edu

Authors

Charis Amber Roberts – Department of Chemistry, University of California, Berkeley, California 94720, United States; Department of Chemistry, Reed College, Portland, Oregon 97202, United States.

Bohyun Park – Department of Chemistry, University of California, Berkeley, California 94720, United States; Department of Chemistry, Korea Advanced Institute of Science and Technology (KAIST), Daejeon 34141, Republic of Korea.

Li-Ping Xu – Cherry L. Emerson Center for Scientific Computation, and Department of Chemistry, Emory University, Atlanta, Georgia 30322, United States.

Jose B. Roque – Department of Chemistry, University of California, Berkeley, California 94720, United States.

Charles S. Yeung – Disruptive Chemistry Fellow, Department of Discovery Chemistry, Merck & Co., Inc., 33 Avenue Louis Pasteur, Boston, Massachusetts 02115, United States.

ACKNOWLEDGMENTS

C. A. R. thanks the Reed College Marsh Cronyn Fellowship for partial funding. B. P. thanks Prof. Mu-Hyun Baik (Institute for Basic Science, Korea Advanced Institute of Technology) for financial support (IBS-R10-A1). R. L. L. thanks Reed College for startup funds. C. S. Y. thanks the Disruptive Chemistry Fellowship program of Merck & Co., Inc., Kenilworth, NJ, USA for support. D. G. M. and L.-P. X. gratefully acknowledge the use of the resources of the Cherry Emerson Center for Scientific Computation at Emory University. D. G. M. thanks the National Science Foundation under the CCI Center for Selective C–H Functionalization (CHE-1700982). L.-P. Xu acknowledges the Natural Science Foundation of China (NSFC 21702126) and the China Scholarship Council for support. R.S. thanks the NIGMS (R35 GM130345A) for support of the portion of the work conducted at Berkeley. We thank Dr. Hasan Celik and UC Berkeley's NMR facility in the College of Chemistry (CoC-NMR) for spectroscopic assistance. Instruments in CoC-NMR are supported in part by NIH S10OD024998. We acknowledge the Catalysis Facility of Lawrence Berkeley National Laboratory, which is supported by the Director, Office of Science, of the U.S. Department of Energy under Contract No. DE-AC02- 05CH11231 for use of resources. We thank Dr. Nick Settineri (UC Berkeley) for assistance with X-Ray crystallographic data acquisition.

REFERENCES

(1) Mitchell, E. A.; Peschiulli, A.; Lefevre, N.; Meerpoel, L.; Maes, B. U. W. Direct α-Functionalization of Saturated Cyclic Amines. *Chem. – Eur. J.* **2012**, *18* (33), 10092–10142.

(2) Vitaku, E.; Smith, D. T.; Njardarson, J. T. Analysis of the Structural Diversity, Substitution Patterns, and Frequency of Nitrogen Heterocycles among U.S. FDA Approved Pharmaceuticals. *J. Med. Chem.* **2014**, *57* (24), 10257–10274.

(3) Drews, J. Drug Discovery: A Historical Perspective. *Science* **2000**, *287* (5460), 1960–1964.

(4) Godula, K.; Sames, D. C-H Bond Functionalization in Complex Organic Synthesis. *Science* **2006**, *312* (5770), 67–72.

(5) Prokopcová, H.; Bergman, S. D.; Aelvoet, K.; Smout, V.; Herrebout, W.; Van der Veken, B.; Meerpoel, L.; Maes, B. U. W. C-2 Arylation of Piperidines through Directed Transition-Metal-Catalyzed sp^3 C–H Activation. *Chem. – Eur. J.* **2010**, *16* (44), 13063–13067.

(6) Jain, P.; Verma, P.; Xia, G.; Yu, J.-Q. Enantioselective Amine α-Functionalization via Palladium-Catalysed C–H Arylation of Thioamides. *Nat. Chem.* **2017**, *9* (2), 140–144.

(7) Verma, P.; Richter, J. M.; Chekshin, N.; Qiao, J. X.; Yu, J.-Q. Iridium(I)-Catalyzed α-C(sp^3)–H Alkylation of Saturated Azacycles. *J. Am. Chem. Soc.* **2020**, *142* (11), 5117–5125.

(8) Jiang, H.-J.; Zhong, X.-M.; Yu, J.; Zhang, Y.; Zhang, X.; Wu, Y.-D.; Gong, L.-Z. Assembling a Hybrid Pd Catalyst from a Chiral Anionic CoIII Complex and Ligand for Asymmetric C(sp^3)–H Functionalization. *Angew. Chem. Int. Ed.* **2019**, *58* (6), 1803–1807.

(9) Greßies, S.; Klauck, F. J. R.; Kim, J. H.; Daniliuc, C. G.; Glorius, F. Ligand-Enabled Enantioselective C –H Activation of Tetrahydroquinolines and Saturated Aza-Heterocycles by RhI. *Angew. Chem. Int. Ed.* **2018**, *57* (31), 9950–9954.

(10) Roque, J. B.; Kuroda, Y.; Jurczyk, J.; Xu, L.-P.; Ham, J. S.; Göttemann, L. T.; Roberts, C. A.; Adpressa, D.; Saurí, J.; Joyce, L. A.; Musaev, D. G.; Yeung, C. S.; Sarpong, R. C–C Cleavage Approach to C–H Functionalization of Saturated Aza-Cycles. *ACS Catal.* **2020**, *10* (5), 2929–2941.

(11) Xu, L.-P.; Roque, J. B.; Sarpong, R.; Musaev, D. G. Reactivity and Selectivity Controlling Factors in the Pd/Dialkylbiarylphosphine-Catalyzed C–C Cleavage/Cross-Coupling of an N-Fused Bicyclo α-Hydroxy-β-Lactam. *J. Am. Chem. Soc.* **2020**, *142* (50), 21140–21152.

(12) Anslyn, E. V.; Dougherty, D. A. *Modern Physical Organic Chemistry*; University Science Books, 2006.

(13) Aoyama, H.; Hasegawa, T.; Omote, Y. Solid State Photochemistry of N,N-Dialkyl-.Alpha.-Oxoamides. Type II Reactions in the Crystalline State. *J. Am. Chem. Soc.* **1979**, *101* (18), 5343–5347..

(14) Oelgemöller, M.; Hoffmann, N. Studies in Organic and Physical Photochemistry – an Interdisciplinary Approach. *Org. Biomol. Chem.* **2016**, *14* (31), 7392–7442.

(15) Griesbeck, A. G.; Heckroth, H. Stereoselective Synthesis of 2-Aminocyclobutanols via Photocyclization of α-Amido Alkylaryl Ketones: Mechanistic Implications for the Norrish/Yang Reaction. *J. Am. Chem. Soc.* **2002**, *124* (3), 396–403.

(16) Sinicropi, A.; Barbosa, F.; Basosi, R.; Giese, B.; Olivucci, M. Mechanism of the Norrish–Yang Photocyclization Reaction of an Alanine Derivative in the Singlet State: Origin of the Chiral-Memory Effect. *Angew. Chem. Int. Ed.* **2005**, *44* (16), 2390–2393.

(17) Kohlschütter, V.; Haenni, P. Zur Kenntnis des Graphitischen Kohlenstoffs und der Graphitsäure. *Z. Für Anorg. Allg. Chem.* **1919**, *105* (1), 121–144.

(18) Ham, J. S.; Park, B.; Son, M.; Roque, J. B.; Jurczyk, J.; Yeung, C. S.; Baik, M.-H.; Sarpong, R. C–H/C–C Functionalization Approach to N-Fused Heterocycles from Saturated Azacycles. *J. Am. Chem. Soc.* **2020**, *142* (30), 13041–13050.

(19) Seeman, J. I. Effect of Conformational Change on Reactivity in Organic Chemistry. Evaluations, Applications, and Extensions of Curtin-Hammett Winstein-Holness Kinetics. *Chem. Rev.* **1983**, *83* (2), 83–134.

(20) Seeman, J. I. The Curtin-Hammett Principle and the Winstein-Holness Equation: New Definition and Recent Extensions to Classical Concepts. *J. Chem. Educ.* **1986**, *63* (1), 42.

(21) Wang, D.; Miao, L.; Feng, L.; Yao, Q.; Mkrtchyan, G.; Crowe, W. E.; Nesterov, E. E.; Wang, Y.; Zhang, X.; Yu, P. Mechanism and Origin of Stereoselectivity in Robinson Annulations Leading to Bicyclo[3.3.1]Nonanes: A Rare Curtin–Hammet Scenario. *J. Phys. Org. Chem.* **2017**, *30* (1), e3595.

(22) Morokuma, K. Molecular Orbital Studies of Hydrogen Bonds. III. C=O···H–O Hydrogen Bond in $H_2CO\cdots H_2O$ and $H_2CO\cdots 2H_2O$. *J. Chem. Phys.* **1971**, *55* (3), 1236–1244.

(23) Ziegler, T.; Rauk, A. On the Calculation of Bonding Energies by the Hartree Fock Slater Method. *Theor. Chim. Acta* **1977**, *46* (1), 1–10.

(24) Parr, R.G.; Yang, W. Density Functional Theory of Atoms and Molecules. Oxford University Press: New York, **1989**.

(25) Bochevarov, A.D.; Harder, E.; Hughes, T. F.; Greenwood, J. R.; Braden, D. A.; Philipp, D. M.; Rinaldo, D.; Halls, M. D.; Zhang, J.; Friesner, R. Jaguar : A high-performance quantum chemistry software program with strengths in life and materials sciences. *Int. J. Quantum Chem.* **2013**, *113*, 2110.

(26) Slater, J. C. Quantum Theory of Molecules and Solids, Vol. 4: The Self-Consistent Field for Molecules and Solids. McGraw-Hill: New York, **1974**.

(27) Vosko, S. H.; Wilk, L.; Nusair, M. Accurate spin-dependent electron liquid correlation energies for local spin density calculations: a critical analysis. *Can. J. Phys.* **1980**, *58*, 1200.

(28) Becke, A. D. Density-functional exchange-energy approximation with correct asymptotic behavior. *Phys. Rev. A* **1988**, *38*, 3098.

(29) Lee, C.; Yang, W.; Parr, R. G. Development of the Colle-Salvetti correlation-energy formula into a functional of the electron density. *Phys. Rev. B* **1988**, *37*, 785.

(30) Becke, A. D. Density-functional thermochemistry. III. The role of exact exchange. *J. Chem. Phys*. **1993**, *98*, 5648.

(31) Grimme, S.; Antony, J.; Ehrlich, S.; Krieg, S. A consistent and accurate ab initio parametrization of density functional dispersion correction (DFT-D) for the 94 elements H-Pu. *J. Chem. Phys*. **2010**, *132*, 154104.

(32) Ditchfield, R.; Hehre, W. J.; Pople, J. A. Self-Consistent Molecular-Orbital Methods. IX. An Extended Gaussian-Type Basis for Molecular-Orbital Studies of Organic Molecules. *J. Chem. Phys.* **1971**, *54*, 724.

(33) Hehre, W. J.; Pople, J. A. Self-consistent molecular orbital methods. XIII. An extended Gaussian-type basis for boron. *J. Chem. Phys.* **1972**, *56*, 4233.

(34) Binkley, J. S.; Pople, J. A. Self-consistent molecular orbital methods. XIX. Split-valence Gaussian-type basis sets for beryllium. *J. Chem. Phys.* **1977**, *66*, 879.

(35) Hariharan, P. C.; Pople, J. A. The influence of polarization functions on molecular orbital hydrogenation energies. *Theor. Chim. Acta* **1973**, *28*, 213.

(36) Hehre, W. J.; Ditchfield, R.; Pople, J. A. Self—Consistent

Molecular Orbital Methods. XII. Further Extensions of Gaussian—Type Basis Sets for Use in Molecular Orbital Studies of Organic Molecules. *J. Chem. Phys.* **1972**, *56*, 2257.

(37) Francl, M. M.; Pietro, W. J.; Hehre, W. J.; Binkley, J. S.; Gordon, M. S.; DeFrees, D. J.; Pople, J. A. Self-consistent molecular orbital methods. XXIII. A polarization-type basis set for second-row elements. *J. Chem. Phys.* **1982**, *77*, 3654.

(38) Hay, P. J.; Wadt, W. R. Ab initio effective core potentials for molecular calculations. Potentials for the transition metal atoms Sc to Hg. *J. Chem. Phys.* **1985**, *82*, 299.

(39) Clark, T.; Chandrasekhar, J.; Spitznagel, G. W.; Schleyer, P. von R. Efficient diffuse function-augmented basis sets for anion calculations. III. The 3-21+G basis set for first-row elements, Li–F. *J. Comput. Chem.* **1983**, *4*, 294.

(40) Frisch, M. J.; Pople, J. A.; Binkley, J. S. Self-consistent molecular orbital methods 25. Supplementary functions for Gaussian basis sets. *J. Chem. Phys.* **1984**, *80*, 3265.

(41) Krishnan, R.; Binkley, J. S.; Seeger, R.; Pople, J. A. Self-consistent molecular orbital methods. XX. A basis set for correlated wave functions. *J. Chem. Phys.* **1980**, *72*, 650.

(42) McLean, A. D.; Chandler, G. S. Contracted Gaussian basis sets for molecular calculations. I. Second row atoms, Z=11–18. *J. Chem. Phys.* **1980**, *72*, 5639.

(43) Marten, B.; Kim, K.; Cortis, C.; Friesner, R. A.; Murphy, R. B.; Ringnalda, M. N.; Sitkoff, D.; Honig, B. New Model for Calculation of Solvation Free Energies: Correction of Self-Consistent Reaction Field Continuum Dielectric Theory for Short-Range Hydrogen-Bonding Effects. *J. Phys. Chem*. **1996**, *100*, 11775.

(44) Friedrichs, M.; Zhou, R. H.; Edinger, S. R.; Friesner, R. A. Poisson−Boltzmann Analytical Gradients for Molecular Modeling Calculations. *J. Phys. Chem. B* **1999**, *103*, 3057.

(45) Edinger, S. R.; Cortis, C.; Shenkin, P. S.; Friesner, R. A. Solvation Free Energies of Peptides: Comparison of Approximate Continuum Solvation Models with Accurate Solution of the Poisson−Boltzmann Equation. *J. Phys. Chem. B* **1997**, *101*, 1190.

(46) Rashin, A. A.; Honig, B. Reevaluation of the Born model of ion hydration. *J. Phys. Chem.* **1985**, *89*, 5588.

TOC Graphic: